European Commission's 7th Framework Programme
Grant Agreement No. **226520**

Project acronym: **COMBINE**

Project full title: **Comprehensive Modelling of the Earth System for Better Climate Prediction and Projection**

Instrument: Collaborative Project & Large-scale Integrating Project

Theme 6: *Environment* Area 6.1.1.4: *Future Climate*

ENV.2008.1.1.4.1: *New components in Earth System modelling for better climate projections*

Start date of project: 1 May 2009 Duration: 48 Months

D7.3: Report on carbon cycle feedback analysis in CMIP5 simulations

Lead work package for this deliverable:
WP7: Climate projections and feedbacks

Organization name of lead contractor for this deliverable: UiB

Due date of deliverable: 31 October 2011
Actual submission date: 4 November 2011

Project co-funded by the European Commission within the Seven Framework Programme (2007-2013)		
Dissemination Level		
PU	Public	X
PP	Restricted to other programme participants (including the Commission Services)	
RE	Restricted to a group specified by the consortium (including the Commission Services)	
CO	Confidential, only for members of the Consortium (including the Commission Services)	

1. Introduction and purpose of the study

The purpose of this study is to evaluate the response strengths in ocean and land biogeochemistry to climate change and to rising atmospheric CO_2. In order to separate the climate and carbon cycle driven responses, Friedlingstein et al. (2003) and Friedlingstein et al. (2006) derived a method to characterize global carbon cycle interactions with climate. This comprises metrics that measure how the climate responds to CO_2, α (K ppm^{-1}), how the land and ocean carbon cycle respond to CO_2, β (GtC ppm^{-1}, split between land and ocean) and how the land and ocean carbon cycle respond to climate change, usually characterised by temperature, γ (GtC K^{-1}, split between land and ocean). Friedlingstein et al. (2006) also defined how to combine these metrics into a single climate-carbon cycle gain factor, g, but Gregory et al. (2009) discuss that the carbon cycle response is better viewed as two strong and opposing feedbacks, both uncertain. The climate-carbon response determines changes in carbon storage due to changes in climate and the concentration-carbon response determines changes in storage due to elevated CO_2.

Unlike physical feedbacks relative to a well known black-body response, the concentration-carbon response is very uncertain, and there is no suitable observation against which to evaluate accurately the climate-carbon cycle gain factor for the next century. Also, these metrics are known to be variable across different scenarios and rates of change (Gregory et al. 2009). Hence any feedback framework should be seen as a technique for assessing relative sensitivities of models and understanding their differences, rather than as an absolute measure of an invariant system property.

The β and γ metrics have been evaluated for the C4MIP models in Friedlingstein et al. 2006 for the SRES-A2 emission scenario. Here, we conduct the same analysis for the idealised CMIP5 1% yr^{-1} model simulations. A disadvantage of the latter setup with prescribed atmospheric CO_2 values is that a feedback of the carbon cycle on climate change is not directly quantifiable. However, due to prescribed atmospheric CO_2 the diagnosed fluxes from the various models for air-sea and air-land CO_2 fluxes can be more easily compared. Since the CMIP5 models performed one additional model simulation, the so-called radiatively coupled run, it is now possible to better assess the validity of the underlying assumption of the method, similar to Gregory et al. (2009).

2. Experiment set up and model description

In this study we follow the approach of Friedlingstein et al. (2003) to separate the impact of rising atmospheric CO_2 levels and of climate change on the modelled CO_2 uptake of land surface and ocean. To this end we use at least two model simulations: A fully coupled (COU) standard simulation with coupled carbon cycle, and an uncoupled simulation (BGC), where the CO_2 is fixed to the preindustrial value in the radiation code of the model. Thereby, the ocean and land components of the models experience rising CO_2 levels while climate change is supressed. The term "climate change" is used in a restricted sense in this approach, since the global mean surface temperature change ΔT is used as a proxy for climate change. Three of the models considered for this report also performed a third simulation, which is similar to the fully coupled simulation, but the land and ocean carbon cycle modules "see" the preindustrial CO_2 level (simulation RAD).

The analysis described here has been applied to 11 C4MIP models run (7 GCMs and 4 EMICs) under the SRES-A2 emission scenario by Friedlingstein et al. (2006). Here we evaluate 4 CMIP5 models (MPI-ESM-LR, HadGEM2-ES, IPSL-CM5A-LR, and CNRM-CM5.1) under the idealised 1% CO_2 increase per year scenario (i.e. atmospheric CO_2 is prescribed, 1%yr^{-1} hereafter). Included in the analysis was also the Bergen Earth System Model (BCM-C), which was run for the 1%yr^{-1} scenario. A description of the C4MIP models can be found in Friedlingstein et al. (2006), which is not repeated here. The five remaining models are briefly described in the following section.

2.1 Model descriptions

2.1.1 BCM-C

The fully coupled Bergen Earth System Model (BCM-C) is an extension of the Bergen Climate Model with an addition of terrestrial (LPJ) and oceanic carbon cycle model (HAMOCC5.1). The physical climate model consists of ARPEGE from Meteo-France and the Miami Isopycnic Coordinate Ocean Model (MICOM). For more details on BCM-C see Tjiputra et al. (2010). MICOM is documented in Bleck and Smith (1990) and Bleck et al. (1992). Updates to the model code are described in Bentsen et al. (2004) and Assmann et al. (2010). With the exception of the equatorial region, the grid configuration employed here is almost regular with a horizontal grid spacing of approximately 2.4°×2.4°. In order to better resolve the dynamics near the equator, the horizontal spacing in the meridional direction is gradually decreased to 0.8 along the Equator. The model has a time step of 4800 seconds and a stack of 34 isopycnic layers in the vertical coordinate, with potential densities ranging from 1029.514 to 1037.800 kg m^{-3}. A non-isopycnic surface mixed layer on top provides the linkage between the atmospheric forcing and the ocean interior.

The current version of HAMMOC (Maier-Reimer et al. 2005) includes an NPZD-type (nutrient, phytoplankton, zooplankton and detritus) ecosystem model following Six and Maier-Reimer (1996). The model contains over 30 biogeochemical tracers, which include dissolved inorganic carbon, total alkalinity, oxygen, nitrate, phosphate, silicate, iron, phytoplankton and zooplankton. Fixed Redfield ratios (i.e., P:N:C:ΔO_2) are used for production and remineralization of biogenic matter. In addition to temperature and light, the phytoplankton growth rate is also co-limited by nitrate, phosphate and iron concentrations. The modelled bulk phytoplankton concentration is divided into diatom and coccolithophore compartments, based on silicate concentration (i.e. higher diatom fraction when the prognostic silicate concentration is high). In the tropical oligotrophic nitrate-depleted regions, the marine ecosystem module accounts for atmospheric nitrogen fixation as for cyanobacteria growth. Particulate organic carbon, produced due to the ecosystem dynamics, is exported out of the euphotic zone with a constant sinking speed. Once exported, the organic matter is remineralized at depth, and the non-remineralized particles are collected by the sediment. The sediment module is based on Heinze et al. (1999) and calculates the same tracers as the water column model. The inorganic carbon chemistry in the model is based on Maier-Reimer and Hasselmann (1987). The surface pCO_2 is computed prognostically as a function of alkalinity, total DIC, temperature, pressure and salinity. The dissolution of calcium carbonate at depth is computed as a function of carbonate ion saturation state and a constant dissolution rate. The air-sea gas (i.e., CO_2 and O_2) exchange processes are formulated as a function of gas solubility, transfer velocity and the difference between partial pressure tracers in air and water.

2.1.2 HadGEM2-ES

HadGEM2-ES (Collins et al. 2011) couples interactive ocean biogeochemistry, terrestrial biogeochemistry and dust, interactive atmospheric chemistry and aerosol components into an update of the physical model HadGEM1 (Johns et al. 2006). The physical model contains a 40 level 1x1 degree, moving to 1/3rd degree at the equator ocean, and a 38 level 1.875 x 1.25 atmosphere (Martin et al. 2011). HadGEM2-ES has been set-up and used to perform all of the CMIP5 simulations as described by Jones et al. (2011).

The ocean biogeochemistry uses the Diat-HadOCC model (Totterdell and Halloran in prep), an update of HadOCC (Palmer and Totterdell 2001), now simulating diatom and non-diatom phytoplankton functional types, a single zooplankton, and cycling of nitrogen, silica and iron. Diat-HadOCC is coupled to other earth system components through the model's physics, iron supplied through dust, air-sea exchange of CO2 and oceanic emission of dimethylsulphide.

The terrestrial carbon cycle is represented by the MOSES2 land surface scheme (Essery et al. 2003) which simulates exchange of water, energy and carbon between the land surface and

the atmosphere, and the TRIFFID dynamic global vegetation model (Cox, 2001) which simulates the coverage and competition between 5 plant functional types (broadleaf tree, needleleaf tree, C3 and C4 grass and shrub) and 4 non-vegetated surface types (bare soil, urban, lakes and land-ice).

2.1.3 IPSL-CM5A-LR

The fifth generation coupled model developed at the IPSL, IPSL-CM5A (IPSLCM5, Dufresne et al. 2011 in prep) consists in the most recent development of the previous version IPSLCM4. It now also includes a module for tropospheric chemistry and aerosols as well as online interactions with both terrestrial and marine biogeochemical carbon cycles.

The atmosphere and land models of IPSLCM5 are updated versions of those used in IPSLCM4, namely, the atmospheric general circulation model LMDZ (Hourdin et al. 2006) and the ORCHIDEE land-surface model (Krinner et al. 2005). The atmospheric and land components use the same horizontal grid that is regular, with 96x96 points and 39 vertical levels representing a resolution of 1.8°x1.8°. There are also twice as many vertical levels as in IPSLCM4. The INCA model is used to simulate tropospheric greenhouses gases and aerosols concentrations, while stratospheric ozone is modeled by REPROBUS. For the oceanic module, IPSLCM5A uses NEMO (Madec 2008), which includes the ocean general ocean circulation model OPA9, the sea ice model LIM (Fichefet and Maqueda 1997), and the oceanic biogeochemistry model PISCES. OPA9 uses a partial-step formulation (Barnier et al. 2006), which ensures a better representation of bottom bathymetry and thus stream flow and friction at the bottom of the ocean. NEMO includes prognostic interaction between incoming shortwave radiation penetration into the ocean and the phytoplankton.

The biogeochemical model PISCES simulates the biogeochemical cycles of oxygen, carbon and the main nutrients that control marine phytoplankton growth: nitrate and ammonium, phosphate, silicate and iron (Aumont and Bopp, 2006). Redfield ratios are constant and phytoplankton growth is limited by the external availability of nutrients. Carbon and nitrogen cycles are decoupled to a certain degree, because PISCES includes nitrogen fixation and denitrification. PISCES has twenty-four tracers. There are five limiting nutrients for phytoplankton growth (nitrate, ammonium, phosphate, silicate and iron). Four living compartments: two phytoplankton size-classes (i.e., nanophytoplankton and diatoms) and two zooplankton size classes (i.e.,microzooplankton and mesozooplankton). There are three non-living compartments: semi-labile dissolved organic matter, small and big sinking particles. The iron, silicon and calcite pools of particles are modeled explicitly. PISCES also simulates dissolved inorganic carbon, total alkalinity and dissolved oxygen.

2.1.4 MPI-ESM-LR

The Max Planck Institute for Meteorology Earth System Model (MPI-ESM-LR) consists of general circulation models for the atmosphere and for the ocean and interactive modules for the marine biogeochemistry and the land biosphere. MPI-ESM-LR thus comprises a fully coupled carbon cycle.

In the atmosphere model ECHAM6, which builds on ECHAM5 (Roeckner et al. 2006), here used in T63L47 resolution, vorticity, divergence, temperature, and the logarithm of surface pressure are represented by truncated series of spherical harmonics. The advection of water vapour, cloud liquid water, and cloud ice are treated by a flux-form semi-Lagrangian scheme. A hybrid sigma/pressure system is used in the vertical direction.

The land surface model JSBACH (Raddatz et al. 2007) is interactively coupled to ECHAM. JSBACH distinguishes several plant functional types (PFTs), including crops and pastures. These PFTs differ with respect to phenology and phptosynthetic productivity, which are computed dynamically in response to climate. JSBACH inherits the modules for photosynthesis and stomatal conductance from the biosphere model BETHY (Knorr 2000) and calculates photosynthesis for C3 plants based on Farquhar et al. (1980) and for C4 plants based on Collatz et al. (1992). Plant carbon is divided into three pools: woody biomass, active

plant tissues such as fine roots and leaves, and a reserve pool for starch and sugars. Above and below ground pools for litter from biomass of living tissues contain easily degradable organic compounds, whereas the above and below ground pools for woody litter degrade at longer time scales. The non-respired fraction of the easily decomposed organic soil and litter material is added to the recalcitrant soil pool of JSBACH. Decomposition is calculated with pool specific fixed turnover rates and regulated exponentially by soil temperature and linearly by soil moisture. The geographic distribution of vegetation is determined dynamically in interaction with climate (Brovkin et al. 2009); land-use change can be either prescribed by sequences of land-use maps (Pongratz et al. 2009), or by prescribing land-use transitions from the land-use protocol by Hurtt et al. (2006).

The ocean model (MPIOM; Marsland et al. 2003) uses the primitive equations for a hydrostatic Boussinesq fluid with a free surface. The vertical discretization is on 40 z-levels, and the bottom topography is resolved by means of partial grid cells. MPIOM applies a conformal mapping grid with a horizontal resolution ranging from 11 km to 150 km with increased resolution in the North Atlantic. It includes a thermodynamic-dynamic sea-ice model with viscous-plastic rheology that considers also snow on sea ice. The marine carbon cycle model HAMOCC5 (Six and Maier-Reimer 2006) is driven by the physical fields of MPIOM and the carbon fluxes are exchanged with ECHAM. Please refer to section 2.1.1 for a description of HAMOCC5.

2.1.5 CNRM-CM5.1

The CNRM-CM5.1 model (CNRMCM5, Voldoire et al. 2011 in revision) also couples atmosphere, land, ocean and sea-ice components. The atmospheric component is ARPEGE-CLIMATv5.2, which has derived from ARPEGE (Déqué et al., 1994). ARPEGE-CLIMATv5.2 is a spectral model using a resolution of about 1.4° in longitude and latitude, while vertically there are 31 levels. The land-surface component is SURFEX (Manzi and Planton 1994, Noilhan and Mahfouf 1996), which prognostically simulates three types of surfaces: land surfaces, free water bodies, ocean or seas. The atmospheric chemistry in CNRMCM5 is reduced to the stratospheric ozone chemistry (MOBIDIC, Cariolle and Teyssèdre, 2007). The ocean component uses NEMOv3.2 in the ORCA1 configuration, which offers 1° to 1/3° horizontal resolution and a vertical discretization of 42 levels. This configuration accounts for an improved Turbulent Kinetic Energy (TKE) closure scheme (Madec 2008), based on the Blanke and Delecluse (1993) TKE. This parametrization allows a fraction of surface wind energy to penetrated bellow the base of the mixed layer depth ensuring a better coupling between surface wind and mixed layer depth. The sea-ice model is GELATO (Salas-Mélia 2002). It simulates four ice thickness categories: 0-0.3 m, 0.3-0.8 m, 0.8-3 m and over 3 m.

The biogeochemical model PISCES (Aumont and Bopp 2006) simulates the biogeochemical cycles of oxygen, carbon and the main nutrients: nitrate and ammonium, phosphate, silicate, iron, two sizes of phytoplankton, two sizes of zooplankton, semilabile dissolved organic matter, small and big sinking particles. Carbon compartment is represented by dissolved inorganic carbon, alkalinity and calcite. For carbon and oxygen pools, air-sea exchange follows the Wanninkhof (1992) formulation.

2.2 Methods

The Friedlingstein et al. (2003) approach rests on three assumptions:

(i) The total change in carbon storage by ocean and land ΔC is a linear combination of changes due to rising atmospheric CO_2 and due to climate change, i.e.

$$\Delta C = \Delta C_{CO2} + \Delta C_{Clim}.$$

(ii) The change in carbon storage due to increasing atmospheric CO_2 is a linear function of atmospheric CO_2 concentration,

$$\Delta C_{CO2} = \beta \, \Delta CO_2.$$

(iii) The change in carbon storage due to climate change is a linear function of temperature change ΔT,

$$\Delta C_{Clim} = \gamma \, \Delta T.$$

These assumptions apply for the land and ocean components separately, that is, we define coefficients β_L, γ_L, and β_O, γ_O for land (subscript L) and ocean (subscript O), respectively. Since assumption (i) has been questioned in a recent publication by Gregory et al. (2009), we investigate the validity of (i) for the three models which performed the RAD simulation. Further we note that Gregory et al. (2009) also demonstrated that assumption (ii) is not necessarily valid across different CO_2 emission/forcing scenarios. They obtained different values for the β-factor under 0.5%, 1% and 2% annual increase in CO_2 for the HadCM3LC and the IPSL-CM4-LOOP models. Despite these methodological pitfalls the analysis performed here can be useful to investigate and compare the characteristics of different models with respect to the carbon cycle.

For this study we use the different model simulations COU, BGC and RAD (only three models) to estimate the β- and γ-factors. Since for the simulations BGC $\Delta T \approx 0$, we have

$$\Delta C^{bgc} = \beta^{bgc} \, \Delta CO_2. \qquad (1)$$

In order to calculate γ, the difference in carbon uptake between the COU and BGC simulation is needed:

$$\Delta C^{cou} = \beta^{cou} \, \Delta CO_2{}^{cou} + \gamma^{cou} \, \Delta T^{cou}$$
$$\Delta C^{bgc} = \beta^{bgc} \, \Delta CO_2{}^{bgc}$$

Assuming that β takes the same value for the coupled and uncoupled run we have

$$\Delta C^{cou} - \Delta C^{bgc} = \beta(\Delta CO_2{}^{cou} - \Delta CO_2{}^{bgc}) + \gamma^{cou} \, \Delta T^{cou} \qquad (2)$$

If a scenario with prescribed atmospheric CO_2 is used, $\Delta CO_2{}^{cou} - \Delta CO_2{}^{bgc} = 0$ and γ^{cou} can be estimated directly from (2). Otherwise, β must be used to correct for the different CO_2 pathways encountered in the coupled und uncoupled simulations (the first term on the right hand side of equation 2). For those models, which have performed the RAD simulation, there is the possibility to calculate another estimate of γ. It is

$$\Delta C^{rad} = \gamma^{rad} \, \Delta T^{rad}, \qquad (3)$$

since the ocean and land carbon cycle modules "see" no increase in atmospheric CO_2 in this kind of simulation.

3. Analysis of idealised 1%yr^{-1} model runs

We will first discuss some general aspects of this analysis here, using the 1%yr^{-1} scenario (5 model runs available). The atmospheric CO_2 concentration and the global mean surface temperature are shown in Figure 1 for the five models BCM-C, MPI-ESM-LR, HadGEM2-ES, IPSL-CM5A-LR, and CNRM-CM5.1. All models show a surface temperature increase of about 5° in the 140 year period. Figure 1c shows the models' climate sensitivity to CO_2, α^{cou}, which is a linear estimate of the change in surface temperature due to changing atmospheric

CO_2 in the fully coupled run. All five models show similar values of α^{rad} in the range 0.0054-

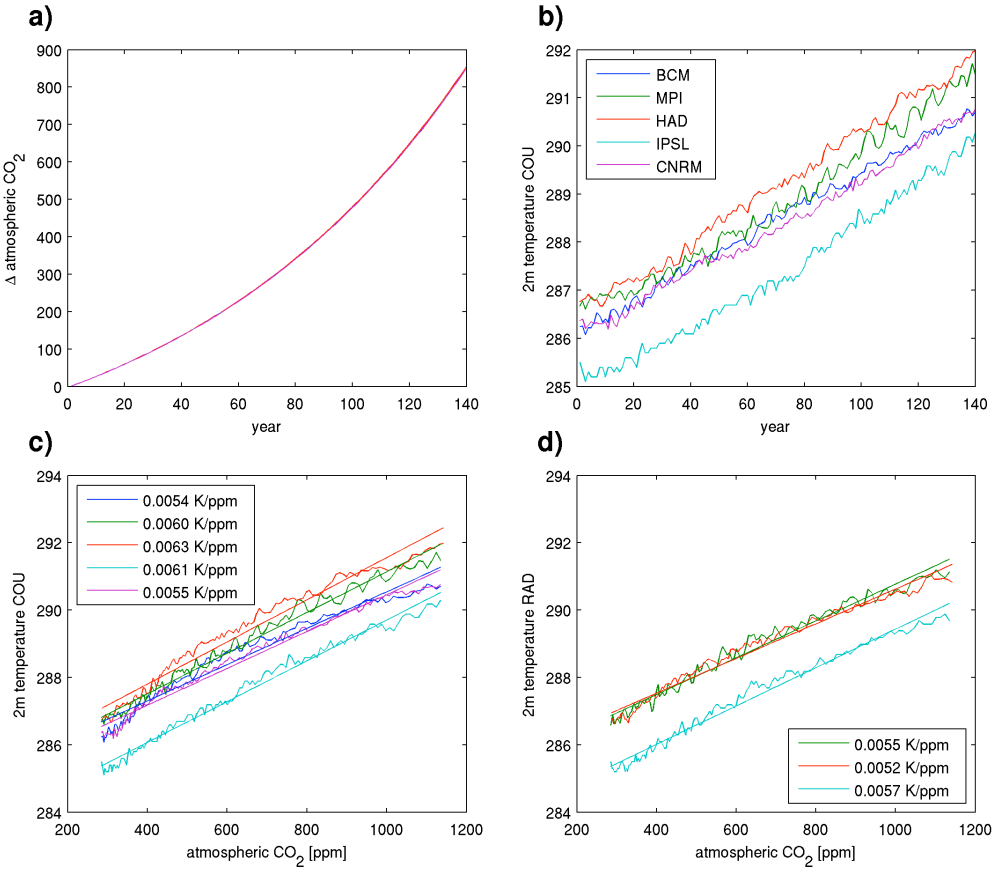

Figure 1: (a) atmospheric CO_2 and (b) global mean 2-m temperature for the COU simulation for the four models which run the 1%yr^{-1} scenario. (c) as (b) but plotted relative to atmospheric CO_2. (d) as (c) but for the RAD simulation. The fitted straight lines are an estimate of the models climate sensitivity α^{cou} (panel c) and α^{rad} (panel d), the values of which are given in the legend.

0.0063 K/ppm (see also Table 1). For the three models that performed the additional RAD simulation (MPI-ESM-LR, HadGEM2-ES, and IPSL-CM5A-LR), the climate sensitivity for the RAD run, α^{rad}, is shown in Figure 1d. The latter sensitivities are smaller by 0.0004 to 0.0009 K/ppm for the individual models. An increase in surface temperature can also be observed in uncoupled BGC simulations (not shown), which is consistent with the observation $\alpha^{rad} < \alpha^{cou}$. The temperature trends in the BGC simulations violate the assumption $\Delta T^{bgc}=0$ needed to estimate β to some extent. However, the temperature increase in the BGC simulations is smaller than 0.26°/100 years except for the HadGEM2-ES model, which shows a warming of approximately 0.5°/100 years. The reason for the differences in α^{rad} and α^{cou} as well as for the temperature trend in the BGC simulations might be the physiological response of stomatal closure to elevated CO_2 levels as discussed in Gregory et al. (2009). Surface temperature trends in the BGC simulations might also arise due to changing land cover properties.

The accumulated carbon uptake relative to atmospheric CO_2 concentration for the BGC simulation is displayed in Figure 2a and Figure 3a for land and ocean, respectively. All models show a small but clearly visible deviation from a linear dependence of ΔC^{bgc} on ΔCO_2, which is generally more pronounced for land carbon uptake. Although climate change is not acting on the carbon cycle in the BGC simulations, this nonlinearity shows up as a tendency to lessen the increase of carbon uptake towards the end of the simulation period. Further, the spread among models is much larger for the land carbon uptake, reaching a difference of approximately 500 Gt of carbon at the end of the BGC simulations. In contrast, the respective

difference for the ocean uptake is less than 180 Gt carbon. The β factors estimated according to equation (1) are summarised in Table 1 and range from 1.04 to 1.63 Gt/ppm for land and 0.77 to 0.94 Gt/ppm for ocean carbon uptake.

Figures 2b and 3b show the difference in accumulated carbon uptake between the COU and BGC simulation plotted relative to the global mean 2m-temprature as a proxy for climate change. Here, the relation between ΔC^{cou} - ΔC^{bgc} and ΔT is only approximately linear. The uptake curves are flatter at lower temperatures and tend to be steeper at higher temperatures for all models and for both, land and ocean uptake. Nevertheless, a linear estimate of γ^{cou} has been calculated for each model according to equation (2). Values of γ^{cou} are given in Table 1. For the three models that performed the additional RAD simulation, accumulated carbon uptake is plotted in Figures 2c and 3c, and γ^{rad} estimated according to equation (3) is given in Table 1. We note that by visual inspection of Figures 2b and 2c as well as 3b and 3c, the assumption of a linear relationship between ΔC^{rad} and ΔT seems to be better justified than assuming a linear ΔC^{cou} - ΔC^{bgc}, ΔT dependence.

Table 1: α^{cou}, α^{rad} [K/ppm], β [Gt/ppm], γ^{cou} and γ^{rad} [Gt/K] for the 1%yr^{-1} scenario

	α^{cou}	α^{rad}	β_L	β_O	γ_L^{cou}	γ_O^{cou}	γ_L^{rad}	γ_O^{rad}
BCM	0.0054	-	1.04	0.87	-99.7	-14.4	-	-
MPI	0.0060	0.0055	1.63	0.89	-82.7	-17.1	-82.8	-8.7
Had	0.0063	0.0052	1.27	0.85	-45.0	-18.4	-21.1	-7.5
IPSL	0.0061	0.0057	1.23	0.94	-38.5	-16.4	-54.7	-10.7
CNRM	0.0055	-	-	0.77	-	-25.4	-	-

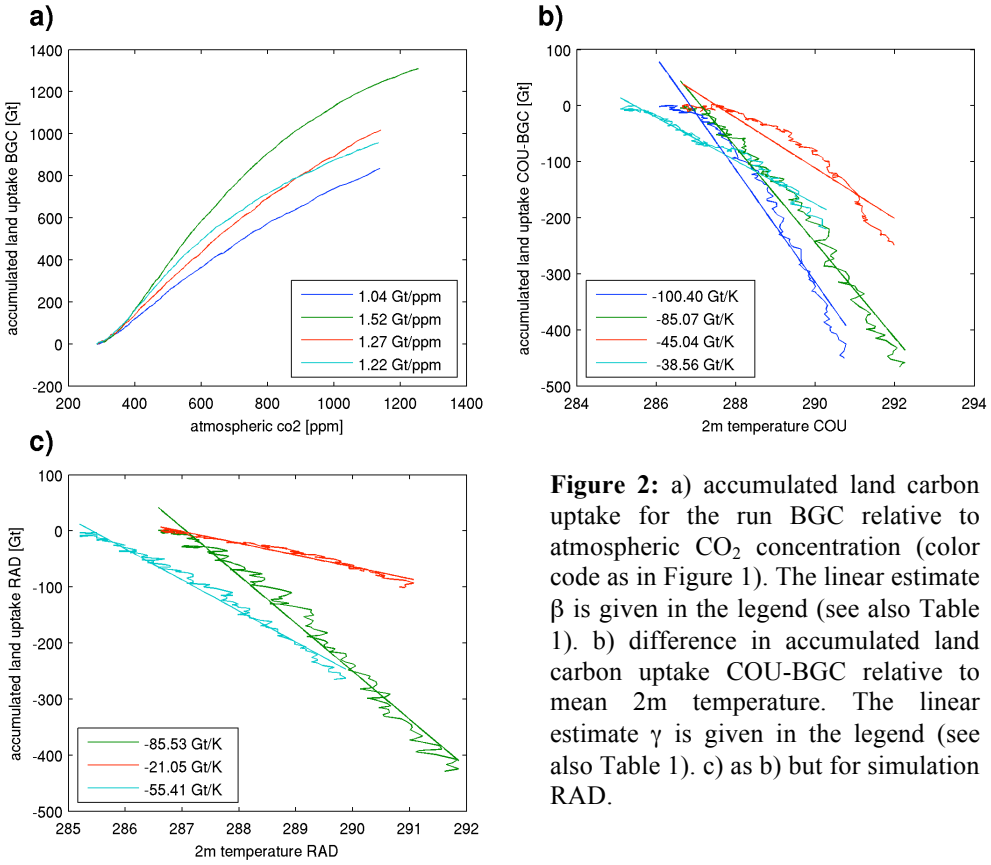

Figure 2: a) accumulated land carbon uptake for the run BGC relative to atmospheric CO_2 concentration (color code as in Figure 1). The linear estimate β is given in the legend (see also Table 1). b) difference in accumulated land carbon uptake COU-BGC relative to mean 2m temperature. The linear estimate γ is given in the legend (see also Table 1). c) as b) but for simulation RAD.

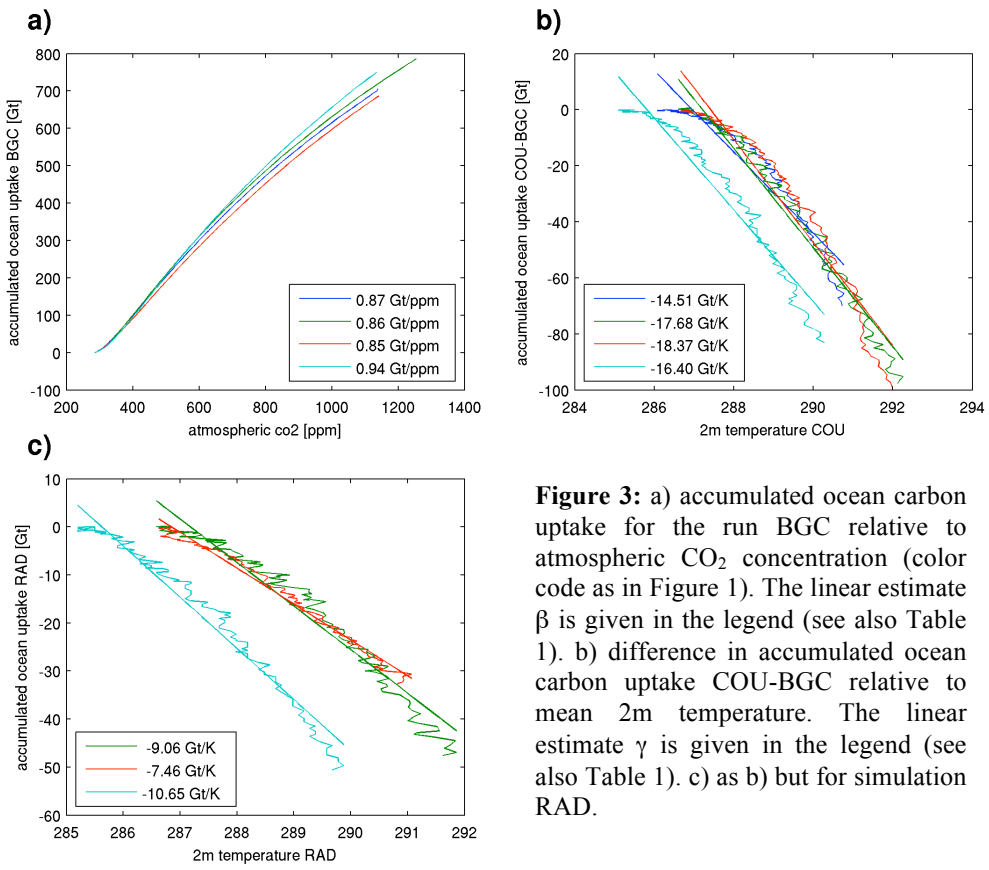

Figure 3: a) accumulated ocean carbon uptake for the run BGC relative to atmospheric CO_2 concentration (color code as in Figure 1). The linear estimate β is given in the legend (see also Table 1). b) difference in accumulated ocean carbon uptake COU-BGC relative to mean 2m temperature. The linear estimate γ is given in the legend (see also Table 1). c) as b) but for simulation RAD.

Generally the two estimates of the carbon uptake climate sensitivity γ^{cou} and γ^{rad} differ considerably. Clearly, the differences are too large to be explained by inaccuracies inherent to the linear fit to not strictly linear data. An exception is the value of γ_L derived from the MPI-ESM-LR model, where both estimates γ_L^{cou} and γ_L^{rad} are similar. In order to better understand these large discrepancies between γ^{cou} and γ^{rad} it is necessary to revisit the validity of assumption (i), i.e., the assumption that the change in carbon uptake is a linear combination of changes induced by rising CO_2 and by climate change (temperature change). The accumulated carbon uptake for the three models with the RAD simulation available is summarised in Figure 4 (land) and Figure 5 (ocean). The figures show the uptake for the COU, BGC, RAD simulations as well as the sum BGC+RAD. According to assumption (i) the latter sum should equal the uptake observed in the COU runs, since the BGC run isolates the impact of rising atmospheric CO_2 while the RAD run represents the influence of increasing temperature. However, as seen in Figure 4, the land carbon uptake in the fully coupled simulation differs from the sum of the biogeochemically and radiatively coupled simulations. While for two models the sum is lager by 37 and 148 Gt carbon (MPI-ESM-LR and HadGEM2-ES, respectively), for IPSL-CM5A-LR model the sum is smaller by approximately 45 Gt. This explains why, for example in the HadGEM2-ES simulations, $|\gamma_L^{rad}|$ is much smaller than $|\gamma_L^{cou}|$. Obviously, in the HadGEM2-ES model, the carbon cycle reacts differently, when climate change and increasing CO_2 are acting simultaneously, leading to less carbon uptake in the COU simulation and thus a larger difference $\Delta C^{cou} - \Delta C^{bgc}$, from which γ^{cou} is estimated. The MPI-ESM-LR model shows the same tendency, though much less pronounced, i.e. the difference between the COU and BGC+RAD carbon uptake is much smaller, leading to $\gamma_L^{rad} \approx \gamma_L^{cou}$ for this model. Interestingly, the ISPL model shows the reverse effect: Here, the BGC+RAD carbon uptake is smaller than in the coupled simulation, leading to $|\gamma_L^{cou}| < |\gamma_L^{rad}|$.

The same analysis for the ocean uptake (Figure 5) reveals that the sum BGC+RAD is

larger than the carbon uptake for the COU simulation in all three models. This means that the uptake in the fully coupled simulation is weaker than expected from the biogeochemically and radiatively coupled simulation, and hence $|\gamma_O^{cou}| > |\gamma_O^{rad}|$ for all models.

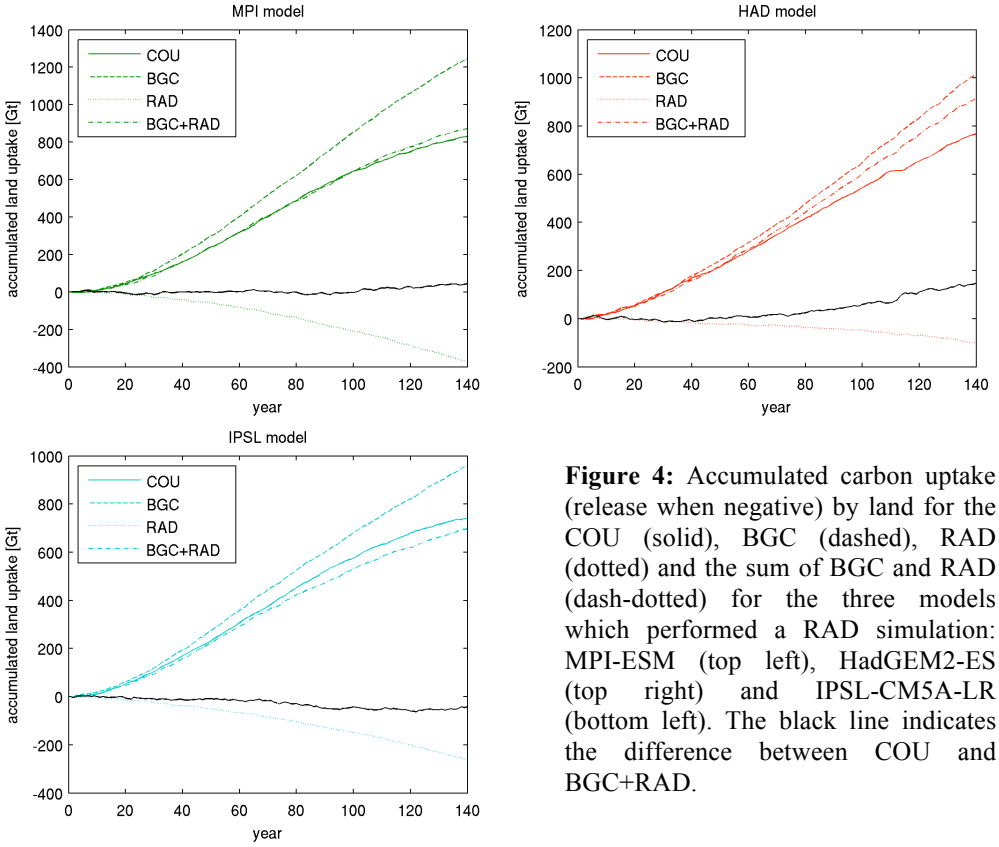

Figure 4: Accumulated carbon uptake (release when negative) by land for the COU (solid), BGC (dashed), RAD (dotted) and the sum of BGC and RAD (dash-dotted) for the three models which performed a RAD simulation: MPI-ESM (top left), HadGEM2-ES (top right) and IPSL-CM5A-LR (bottom left). The black line indicates the difference between COU and BGC+RAD.

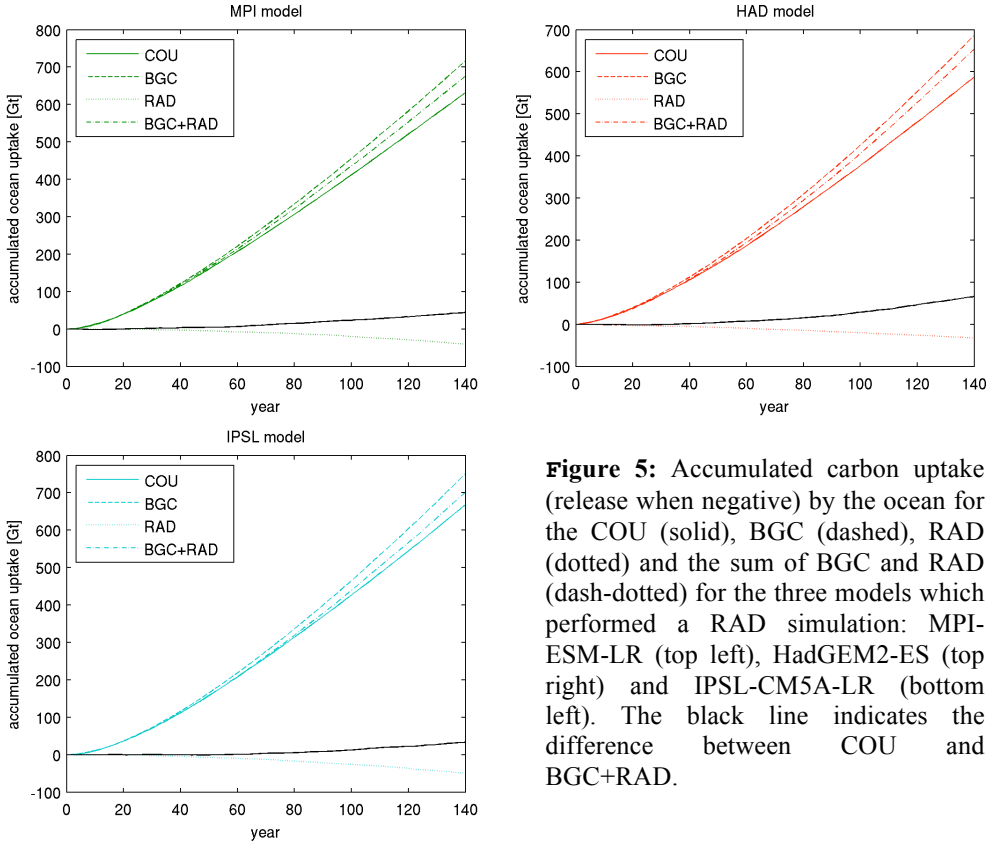

Figure 5: Accumulated carbon uptake (release when negative) by the ocean for the COU (solid), BGC (dashed), RAD (dotted) and the sum of BGC and RAD (dash-dotted) for the three models which performed a RAD simulation: MPI-ESM-LR (top left), HadGEM2-ES (top right) and IPSL-CM5A-LR (bottom left). The black line indicates the difference between COU and BGC+RAD.

4. Intercomparison of CMIP5 with C4MIP results.

The β and γ metrics have been evaluated for the C4MIP and CMIP5 (MPI-ESM-LR, HadGEM2-ES, and IPSL-CM5A-LR) models. For this comparison one additional model, the CanESM (Arora et al. 2011), has been taken into account. Figure 6 compares the α, β, and γ factors separately for land and ocean for the 11 C4MIP models and the four CMIP5 models. The γ-factors presented here are based on equation (2), i.e. γ^{cou}, since no RAD simulations are available for the C4MIP models. We note that all factors given in this section have been calculated according to the C4MIP protocol, where the linear estimates are calculated by taking into account the start and end point of the respective curves. This is slightly different from the approach taken in section 3, where a straight line was fitted through all available data points, and hence the values presented for the CMIP5 models in Figure 6 differ slightly from the values given in section 3. Further, since the C4MIP runs used the SRES-A2 emission scenario while the CMIP5 simulations were carried out using the idealised 1%yr^{-1} scenario, the β and γ factors are not directly comparable, since the models are known to react differently under different CO_2 forcings (Gregory et al. 2009).

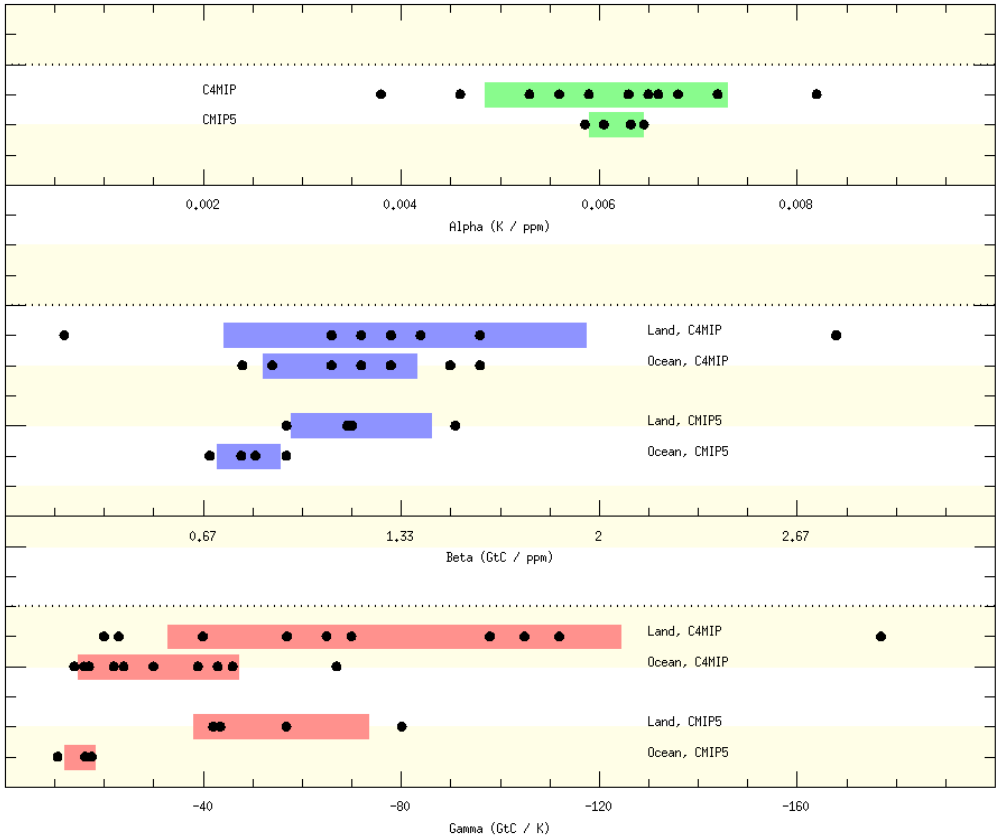

Figure 6: Comparison of carbon cycle feedback metrics between the C4MIP ensemble of 7 GCMs and 4 EMICs (Friedlingstein et al. 2006) and new CMIP5 models (HadGEM2-ES, IPSL, CanESM, MPI-ESM-LR). Black dots represent a single model simulation and coloured bars show the mean +/- 1 standard deviation of the multi-model results.

At this stage, with only 4 CMIP5 models in the comparison it is too early to make definitive comments about whether or not our representation of the climate-carbon cycle system has changed since C4MIP. α, and both β_L and γ_L do not appear statistically distinct in the new CMIP5 multi-model ensemble. The standard deviation is smaller, but this is due to having fewer models. No statements can yet be made about the relative model spread between CMIP5 and C4MIP. For the ocean these metrics appear to be weaker in sensitivity (smaller β_O and γ_O), but that can partly be explained by the use of a different scenario. Particularly for β we would expect the 1%yr^{-1} scenario to yield metrics about 20% smaller than for SRES-A2.

The CMIP5 1% scenario has much faster rising CO_2 than the C4MIP SRES-A2 scenario and as such the ocean cannot respond as quickly, leading to smaller diagnosed beta and gamma metrics. For γ_O the CMIP5 models do appear significantly lower in magnitude, but more CMIP5 results are required before this can be confirmed as a systematic difference since C4MIP.

5. Discussion and conclusion

With the new "radiatively coupled" type simulations available for some of the CMIP5 models, the basis for assessing feedback mechanisms related to the carbon cycle has improved. These simulations have been available from three groups of the COMBINE consortium with the models MIP-ESM, HadGEM3-ES, and IPSL-CM5A-LR. It turns out, that the assumption that the carbon storage is the sum of isolated changes due to rising atmospheric CO_2 and due to climate change is only approximately valid under the $1\%yr^{-1}$ CO_2 scenario. The difference between modelled carbon uptake in the fully coupled simulations and the uptake calculated as the sum from the radiatively and biogeochemicaly coupled simulations amounts to 32-66 Gt carbon (ocean uptake) and -45 to 148 Gt carbon (land uptake) at the end of the 140 year simulation period. These differences correspond to 4.8% to 11.2% (ocean) and -6.0% to 19.3% (land) of the carbon uptake in the fully coupled simulation. Seemingly, the carbon cycle reacts differently under simultaneously rising temperature and CO_2, compared to the synthetic simulations, where only one of the factors is changing. While for the ocean, all models show the same sign of this nonlinear effect, i.e. less uptake in the fully coupled simulation than would be predicted by the sum of radiatively and biogeochemicaly coupled runs, the models disagree on the sign of this non-linearity for land carbon uptake. Since the $1\%yr^{-1}$ has a rather fast rising atmospheric CO_2 (almost three times faster than observed), it would be interesting to repeat this analysis for simulations with a more moderate CO_2 growth once more model simulations have become available.

The carbon uptake by the ocean calculated by the five models, which have run the $1\%yr^{-1}$ simulations, is relatively homogenous. This is reflected in the small spread of β_O (0.77 to 0.94 Gt C/ppm). The models disagree much more in predicting the land carbon uptake, resulting in β_L ranging from 1.04 to 1.63 Gt C/ppm. The same is true for the temperature sensitivity of carbon uptake, represented by γ_O and γ_L. While the for the ocean uptake there is moderate variability in model results with γ_O values between -14.4 and -25.4 Gt C/K, the γ_L values range from -38.5 to -99.6 Gt C/K. Although, as discussed in section 3, the values of γ change, if they are estimated by means of the radiatively coupled simulation, the much smaller spread of γ_O compared to γ_L remains. Although this conclusion is only based on five models so far, it is consistent with the results of the C4MIP model comparison study. Unfortunately, it is too early to conclude whether or not the model spread in general has been reduced for the CMIP5 models compared to C4MIP, before more CMIP5 model results become available.

References

Assmann, K. M., Bentsen, M., Segschneider, J., and Heinze, C.: An isopycnic ocean carbon cycle model, Geosci. Model Dev., 3, 143–167, 2010.

Aumont, O. and Bopp, L.: Globalizing results from ocean in situ iron fertilization studies, Global Biogeochem. Cycles, 20(2), doi:10.1029/2005GB002591, 2006.

Barnier, B. et al.: Impact of partial steps and momentum advection schemes in a global ocean circulation model at eddy-permitting resolution, Ocean Dynamics 56, 543–567, doi :10.1007/s10236-006-0082-1, 2006.

Bentsen, M., Drange, H., Furevik, T., and Zhou, T.: Simulated variability of the Atlantic meridional overturning circulation, Clim. Dynam., 22, 701–720, 2004.

Blanke, B. and Delecluse, P.: Variability of the Tropical Atlantic Ocean Simulated by a General Circulation Model with Two Different Mixed-Layer Physics, J. Phys. Oceanogr., 23(7), 1363–1388, 1993.

Bleck, R. and Smith, L. T.: A wind-driven isopycnic coordinate model of the North and Equatorial Atlantic Ocean, 1. Model development and supporting experiments, J. Geophys. Res., 95, 3273–3285, 1990.

Bleck, R., Rooth, C., Hu, D., and Smith, L. T.: Salinity-driven Thermocline Transients in a Wind- and Thermohaline-forced Isopycnic Coordinate Model of the North Atlantic, J. Phys. Oceanogr., 22, 1486–1505, 1992.

Brovkin, V., T. Raddatz, C. H. Reick, M. Claussen, and V. Gayler: Global biogeophysical interactions between forest and climate, Geophys. Res. Lett., 36, L07405, doi:10.1029/2009GL037543, 2009.

Cariolle, D. and Teyssedre, H.: A revised linear ozone photochemistry parameterization for use in transport and general circulation models: multi-annual simulations, Atmos. Chem. Phys., 7(9), 2183–2196, 2007.

Collatz et al.: Coupled photosynthesis-stomatal conductance model for leaves of C4 plants, Australian Journal Of Plant Physiology 19:519-538, 1992

Collins, W. J., et al.: Development and evaluation of an Earth-system model - HadGEM2, Geosci. Model Dev. Discuss., 4, 997-1062, doi:10.5194/gmdd-4-997-2011, 2011.

Cox, P. M.: Description of the TRIFFID Dynamic Global Vegetation Model, Technical Note 24, Hadley Centre, Met Office, 17 pp., 2001.

Déqué, M., Dreveton, C., Braun, A. and Cariolle, D.: The ARPEGE/IFS atmosphere model: a contribution to the French community climate modelling, Climate Dynamics, 10, 249–266, 1994.

Essery, R. L. H., Best, M. J., Betts, R. A., Cox, P. M., and Taylor, C. M.: Explicit representation of subgrid heterogeneity in a GCM land-surface scheme, J. Hydrometeorol., 43, 530-543, 2003.

Farquhar, G. D., S. Caemmerer and J. A. Berry: A biochemical model of photosynthetic CO2 assimilation in leaves of C3 species, Planta 149: 78-90, 1980.

Fichefet, T. and M. Maqueda: Sensitivity of a global sea ice model to the treatment of ice thermodynamics and dynamics, Geophys. Res. Let. , 102 (C6), 609-646, 1997.

Friedlingstein, P., Dufresne, J.-L., Cox, P. M. and Rayner, P.: How positive is the feedback between climate change and the carbon cycle?. Tellus B, 55: 692–700, doi: 10.1034/j.1600-0889.2003.01461.x, 2003.

Friedlingstein, P., and Coauthors: Climate–Carbon Cycle Feedback Analysis: Results from the C4MIP Model Intercomparison, J. Climate, 19, 3337–3353, doi:10.1175/JCLI3800.1, 2006.

Gregory, J. et al.: Quantifying carbon-cycle feedbacks, J. Climate, 22, 5232-5250, doi10.1175/2009JCLI2949.1, 2009.

Heinze, C., E. Maier-Reimer, A. M. E. Winguth, and D. Archer: A global oceanic sediment model for long-term climate studies, Global Biogeochem. Cycles, 13(1), 221–250, doi:10.1029/98GB02812, 1999.

Hourdin, F. et al.: The LMDZ4 general circulation model: climate performance and sensitivity to parametrized physics with emphasis on tropical convection. Climate Dynamics, 27 (7-8), 787-813, doi:10.1007/s00382-006-0158-0, 2006.

Hurtt, G. C., Frolking, S., Fearon, M. G., Moore, B., Shevliakova, E., Malyshev, S., Pacala, S. W. and Houghton, R. A.: The underpinnings of land-use history: three centuries of global gridded land-use transitions, wood-harvest activity, and resulting secondary lands. Global Change Biology, 12: 1208–1229. doi: 10.1111/j.1365-2486.2006.01150.x, 2006.

Johns, T.C. et al. : The new Hadley Centre climate model HadGEM1: Evaluation of coupled simulations J. Climate, 19(7), 1327-1353, 2006.

Jones, C. D., et al.: The HadGEM2-ES implementation of CMIP5 centennial simulations, Geosci. Model Dev., 4, 543-570, doi:10.5194/gmd-4-543-2011, 2011.

Knorr, W.: Annual and interannual CO2 exchanges of the terrestrial biosphere: process-based simulations and uncertainties. Global Ecology and Biogeography, 9: 225–252. doi: 10.1046/j.1365-2699.2000.00159.x, 2000.

Krinner, G., N. Viovy, N. de Noblet-Ducoudré, J. Ogée, J. Polcher, P. Friedlingstein, P. Ciais, S. Sitch, and I. C. Prentice : A dynamic global vegetation model for studies of the coupled atmosphere-biosphere system, Global Biogeochem. Cycles, 19, GB1015, doi:10.1029/2003GB002199, 2005.

Madec, G. (2008). NEMO ocean engine.Madec, G.: NEMO ocean engine, Note du Pole de modélisation, 321p [online] Available from: http://www.nemo-ocean.eu/About-NEMO/Reference-manuals, 2008.

Maier-Reimer, E. and Hasselmann, K.: Transport and storage of CO2 in the ocean-an inorganic ocean-circulation carbon cycle model, Clim. Dynam., 2, 63–90, 1987.

Maier-Reimer, E., Kriest, I., Segschneuder, J., and Wetzel, P.: The HAMburg Ocean Carbon Cycle Model HAMOCC5.1 – Technical Description Release 1.1, Berichte zur Erdsystemforschung 14, ISSN 1614-1199, Max Planck Institute for Meteorology, Hamburg, Germany, 50 pp., 2005.

Manzi, A. O. and Planton, S.: Implementation of the ISBA parametrization scheme for land surface processes in a GCM — an annual cycle experiment, Journal of Hydrology, 155(3-4), 353–387, doi:10.1016/0022-1694(94)90178-3, 1994.

Marsland, S. J., H. Haak, J. H. Jungclaus, M. Latif, F. Röske: The Max-Planck-Institute global ocean/sea ice model with orthogonal curvilinear coordinates, Ocean Modelling 5, 91-127, 2003.

Martin, G. M. and the HadGEM2 Development Team: The HadGEM2 family of Met Office Unified Model Climate configurations, Geosci. Model Dev. Discuss., 4, 765-841, doi:10.5194/gmdd-4-765-2011, 2011.

Noilhan, J. and Mahfouf, J. F.: The ISBA land surface parameterisation scheme, Global and Planetary Change, 13(1-4), 145–159, doi:10.1016/0921-8181(95)00043-7, 1996

Palmer, J. R. and Totterdell, I. J.: Production and export in a global ocean ecosystem model, Deep Sea Res., Pt. I, 48, 1169-1198, doi:10.1016/S0967-0637(00)00080-7, 2001.

Pongratz, J., C. H. Reick, T. Raddatz, and M. Claussen: Effects of anthropogenic land cover change on the carbon cycle of the last millennium, Global Biogeochem. Cycles, 23, GB4001, doi:10.1029/2009GB003488, 2009.

Raddatz, T. J., C. H. Reick, W. Knorr, J. Kattge, E. Roeckner, R. Schnur, K.-G. Schnitzler, P. Wetzel and J. Jungclaus: Will the tropical land biosphere dominate the climate–carbon cycle feedback during the twenty-first century? Clim. Dyn. 29, 565–574, doi: 10.1007/s00382-007-0247-8, 2007.

Roeckner, E., R. Brokopf, M. Esch, M. Giorgetta, S. Hagemann, and L. Kornblueh: Sensitivity of Simulated Climate to Horizontal and Vertical Resolution in the ECHAM5 Atmosphere Model. J. Climate, 19, 3771–3791, doi: 10.1175/JCLI3824.1, 2006.

Salas-Mélia, D.: A global coupled sea ice-ocean model, Ocean Modelling, 4, 137–172, 2002.

Six, K. D. and E. Maier-Reimer: Effects of plankton dynamics on seasonal carbon fluxes in an ocean general circulation model, Global Biogeochem. Cycles., 10, 559–583, 1996.

Six, K. D. and E. Maier-Reimer: What controls the oceanic dimethylsulfide (DMS) cycle? A modeling approach, Global Biogeochem. Cycles, 20, GB4011, doi:10.1029/2005GB002674, 2006.

Tjiputra, J.F., K. Assmann , M. Bentsen , I. Bethke , O. H. Otterå , C. Sturm , and C. Heinze: Bergen Earth system model (BCM-C): model description and regional climate-carbon cycle feedbacks assessment, Geosci. Model Dev., 3, 123–141, 2010.

Totterdell, I. J. and Halloran, P. R.: Sensitivity of global and regional marine productivity to iron input in a coupled earth system model, Geosci. Model Dev., in preparation, 2011

Voldoire, A., Sanchez-Gomez, E., Salas y Mélia, D., Decharme, B., Cassou, C., Sénési, S., Valke, S., Beau, I. and al, E.: The CNRM-CM5.1 global climate model: Description and basic evaluation, Climate Dynamics, 2011.

Wanninkhof, R.: A relationship between wind speed and gas exchange over the ocean, J. Geophys. Res., 97(C5), 7373–7382, 1992.